Electronic Supplementary Information

In Situ Study of Nucleation and Growth Dynamics of Au Nanoparticles on MoS$_2$ Nanoflakes

Boao Song [1], Kun He [1], Yifei Yuan [1, 2], Soroosh Sharifi-Asl [1], Meng Cheng [1], Jun Lu [2],*

Wissam A. Saidi [3], Reza Shahbazian-Yassar [1*]*

[1] Department of Mechanical and Industrial Engineering, University of Illinois at Chicago, Chicago,

Illinois 60607, USA

[2] Chemical Science and Engineering Division, Argonne National Laboratory, 9700 S. Cass Avenue,

Argonne, Illinois 60439, USA

[3] Department of Mechanical Engineering and Materials Science, University of Pittsburgh, Pittsburgh,

Pennsylvania 15261, USA

* Correspondence to: rsyassar@uic.edu; alsaidi@pitt.edu; junlu@anl.gov

Movie S1 ($\times$2) Nucleation and growth of Au nanoparticles on MoS$_2$ nanoflake.

Movie S2 ($\times$2) Nucleation and growth of Au nanoparticles on MoS$_2$ nanoflake.

Movie S3 ($\times$1) Nucleation and growth of Au nanoparticles on MoS$_2$ with sulfur vacancies.

Supporting Note S1

To analyze the bulging effect of SiN viewing membrane, electron energy loss spectra (EELS) was acquired

from liquid cell that contained the same precursor solution. With a liquid layer thickness of 500 nm at the

window edge, we obtained EELS data at various distance from the window edge. The low-loss EELS data

is shown in Figure S1a. To calculate the corresponding liquid layer thickness, the Beer's law was used to

determine the inelastic mean free path:

$$\frac{t}{\lambda} = ln\left(\frac{I_{tot}}{I_o}\right) \tag{1}$$

here t is sample thickness, λ is inelastic mean free path, I_{tot} and I_o is total spectrum and zero-loss peak

integral, respectively. The λ is determined by the approximation

of

$$\lambda = \frac{106FE_0}{E_M \ln\left(\frac{2\beta E_0}{E_M}\right)} \tag{2}$$

where E_0 is acceleration voltage, F is the relativistic factor at 200 kV,[1] β is the EELS collection semi-

angle, and E_M is the factor related to effective atomic number (Z_{eff}):

$$E_M = 7.6Z_{eff}^{0.36} \tag{3}$$

$$Z_{eff} = \frac{\sum f_n Z_n^{1.3}}{\sum f_n Z_n^{0.3}} \tag{4}$$

where f_n is atomic fraction of element and Z_n is atomic number of element. From these calculations the

liquid layer thickness can be determined and is shown in Figure S1b. It is concluded that the SiN window

bulging effect causes the liquid thickness to increase from 500 nm at the window edge to ~ 975 nm at the

distance of 4 μm away from the window edge.
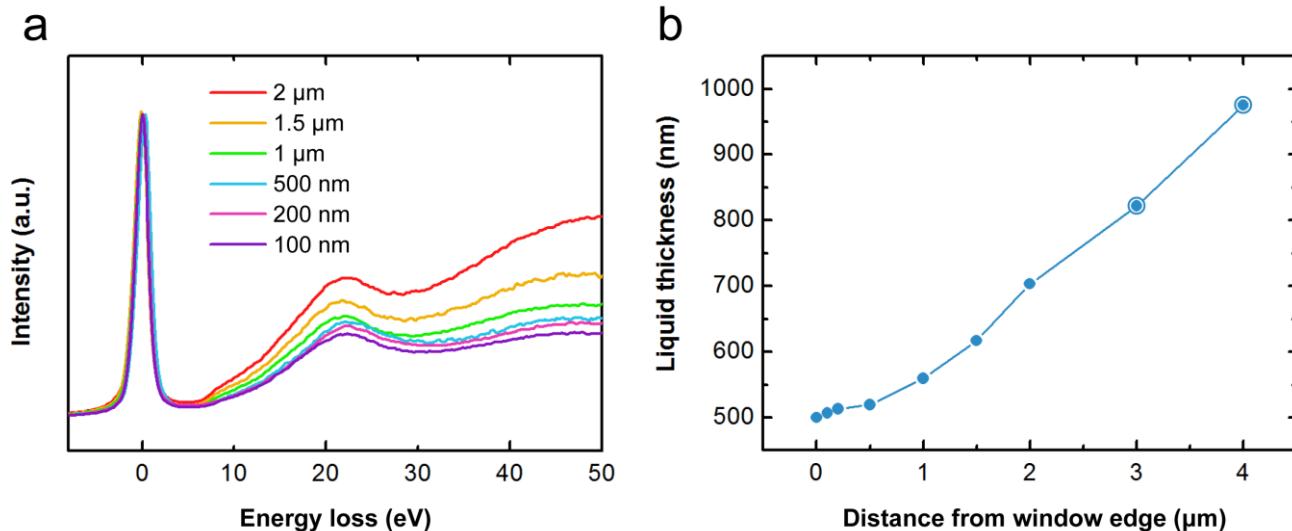
Figure S1. (**a**) Low-loss EELS at different distances from SiN window edge. (**b**) Liquid layer thickness as a function of distance from SiN window edge obtained from the corresponding EELS in **a**.

Supporting Note S2

Particle detection methodology analyzes all the image frames within each video. The exemplary original frame is shown in Figure S2a. First, a bandpass filter was applied to filter large structures down to 40 pixels and small structures up to 3 pixels (Figure S2b). Second, the threshold was adjusted to maximum threshold value of 95 such that segmentation of particles and background can be achieved (Figure S2c). Lastly, the Analyze Particle function in ImageJ was used to detect the outline of particles (Figure S2d).
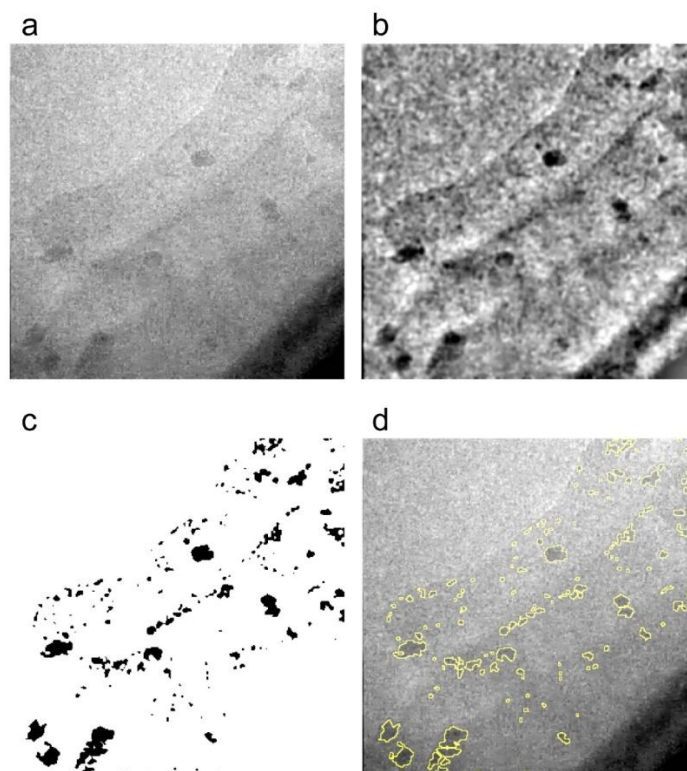
Figure S2. (**a**) An example of a raw frame from Movie S1. (**b**) Bandpass filtered image of **a**. (**c**) Resulted image after threshold adjustment. (**d**) Detected particle outlines overlapped with original frame.
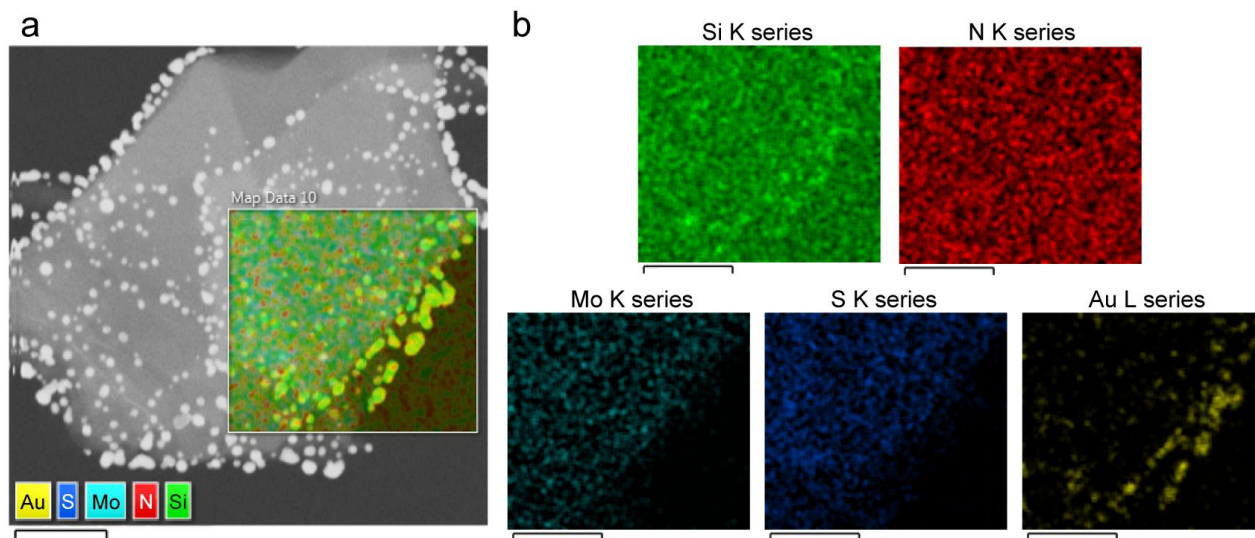
Figure S3. (**a**) EDS mapping of the same area of Figure 4a with signals from SiN viewing window. (**b**) EDS single element mappings for Si, N, Mo, S, and Au. All scale bars are 100 nm.

S4
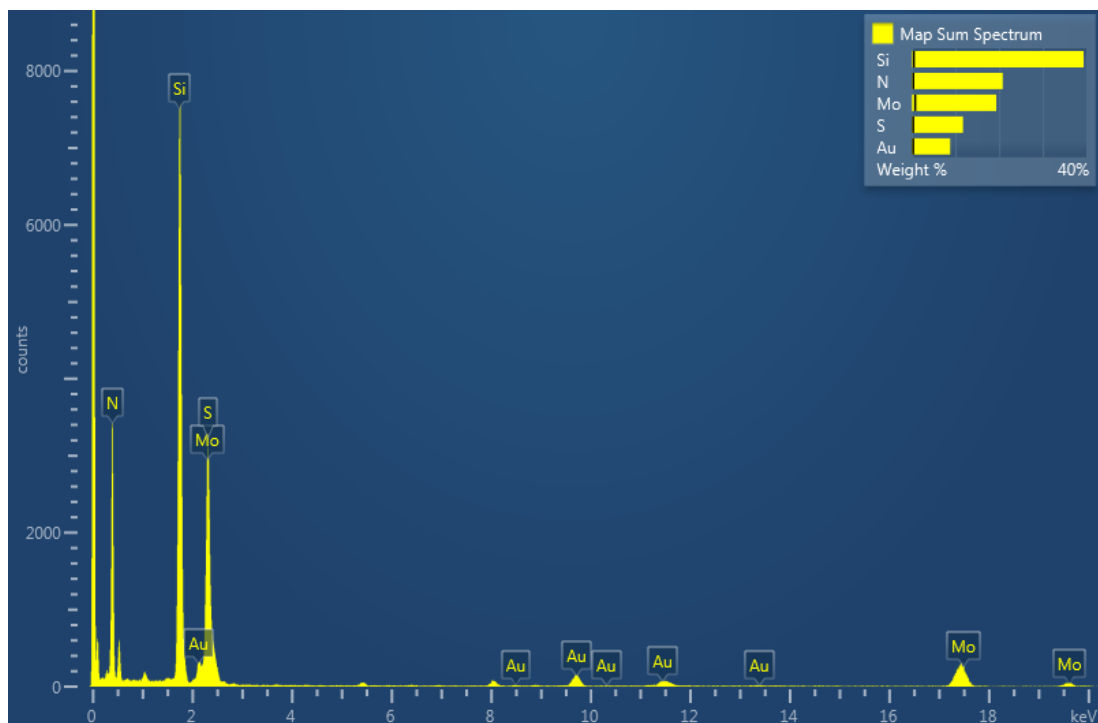
Figure S4. The spectrum corresponding to the EDS mapping in Figure 4a and S3a.

Supporting Note S3

To identify the MoS_2 nanoflakes edges, EELS was involved to measure the relative thickness of MoS_2 surface. Figure S5a shows LAADF image taken at MoS_2 area after *in situ* experiment. The EELS data were acquired along the region marked by red cross symbols. The low-loss EELS data are shown in Figure S5b with a measured inelastic mean free path t/λ of a constant value equal to 0.64. The results suggest that MoS_2 nanoflake is flat in the measured region and no edge on the interior area could be detected. During particle size analysis this method was utilized to examine the existence of step edges on MoS_2 to better distinguish between Au nanoparticles on the edge and interior of the nanoflakes.
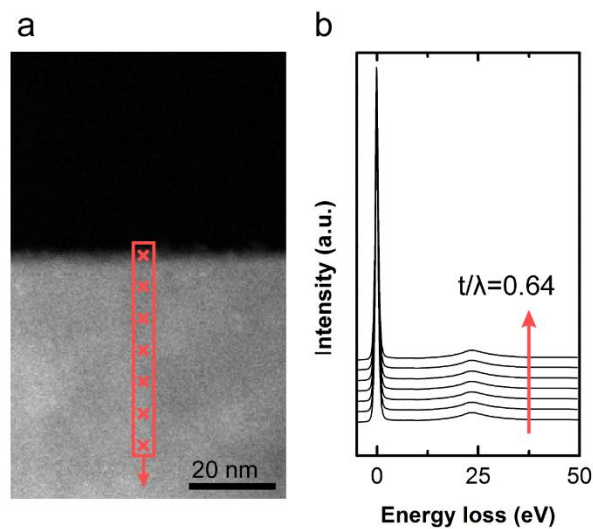
Figure S5. (a) The LAADF image of MoS_2 nanoflake. The red cross symbols mark the region from where the EELS data were acquired. **(b)** Low-loss EELS collected within the region in **a**.
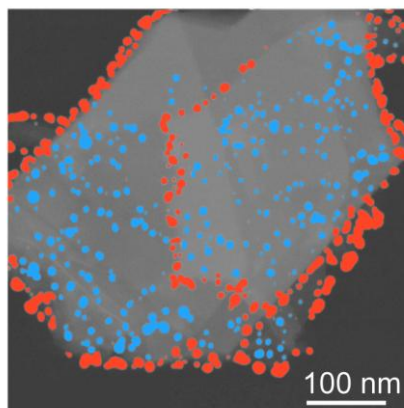
Figure S6. Example image for particle size measurement. The Au nanoparticles marked with blue and red correspond to those formed on MoS_2 interior and along MoS_2 edge.

Supporting Note S4

Electron beam was utilized to create sulfur vacancies on MoS_2 nanoflakes. To further understand the beam effects, the maximum energy (E_{trans}) that can be transferred to an atom is calculated as follows,[2]

S6

$$E_{trans} = \frac{E_{beam}(E_{beam} + 2m_e c^2)}{E_{beam} + \frac{1}{2}Mc^2\left(1 + \frac{m_e}{M}\right)^2} \tag{5}$$

where E_{beam} is the incident electron beam energy from (S)TEM, m_e is the electron rest mass, M is the corresponding atomic mass, and c is the light speed. At specific incident electron beam energy E_{beam}, the atom will be displaced from material surface if the maximum transferred energy E_{trans} exceeds displacement energy, E_d. This knock-on effect caused by electron beam will generate vacancies or induce material damage. Figure S7 shows the relationship between incident electron beam energy (keV) and maximum transferred energy (eV) for sulfur (pink), molybdenum (blue) from MoS_2 as well as pristine gold (yellow). The dashed lines are threshold displacement energies E_d for S (7 eV), Mo (20 eV)[3] and Au (about 40 eV) atoms.[4] For each element, the shadowed area indicates the safe range of electron beam energy that does not induce knock-on effect. In the case of sulfur, the safe range is from zero to about 100 keV, which means that in our 200 keV experimental condition, sulfur atoms are likely to be removed from MoS_2 surface. The safe ranges for Mo and Au are from zero to more than 200 keV due to their relatively high E_d. Thus, the electron beam irradiation only generates sulfur vacancies on MoS_2 surface under our 200 keV experimental condition. A high dose rate of 90 e⁻/(Å²·s) was used to generate sulfur vacancies on MoS_2. After that, all *in situ* experiments were at a low electron dose rate of 50 e⁻/(Å²·s) such that knock-on effect of MoS_2 can be minimized.
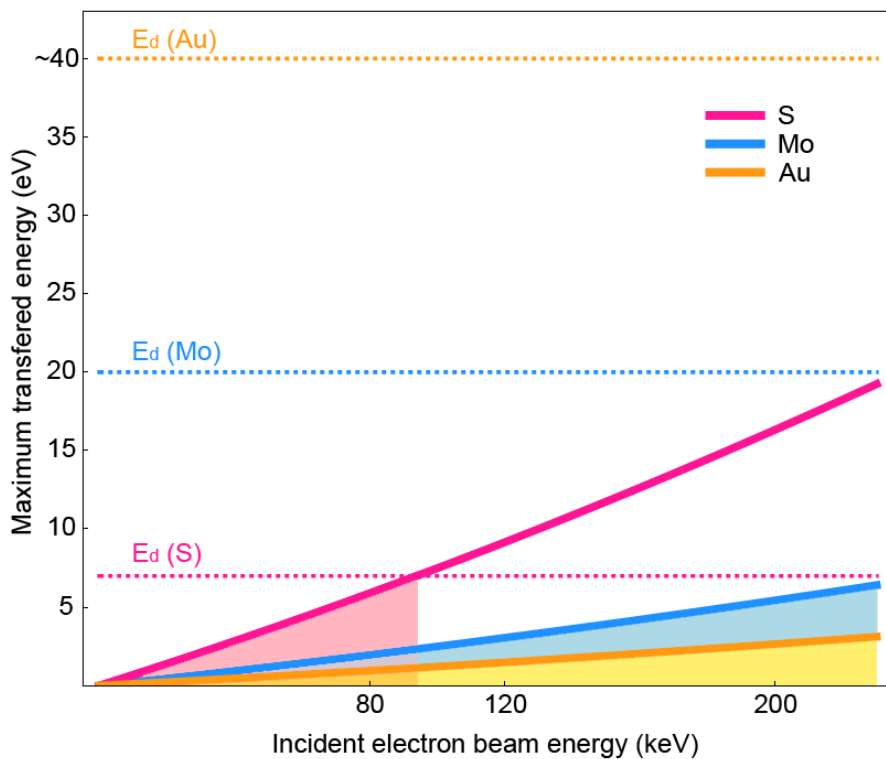
Figure S7. Relationship between incident electron beam energy (keV) and maximum transferred energy (eV) for sulfur (pink), molybdenum (blue) from MoS_2 and pristine gold (yellow). Dashed lines show the threshold displacement energy (E_d) for corresponding elements. Shadow areas show the range of incident electron beam energy that will keep the corresponding elements free of displacement.
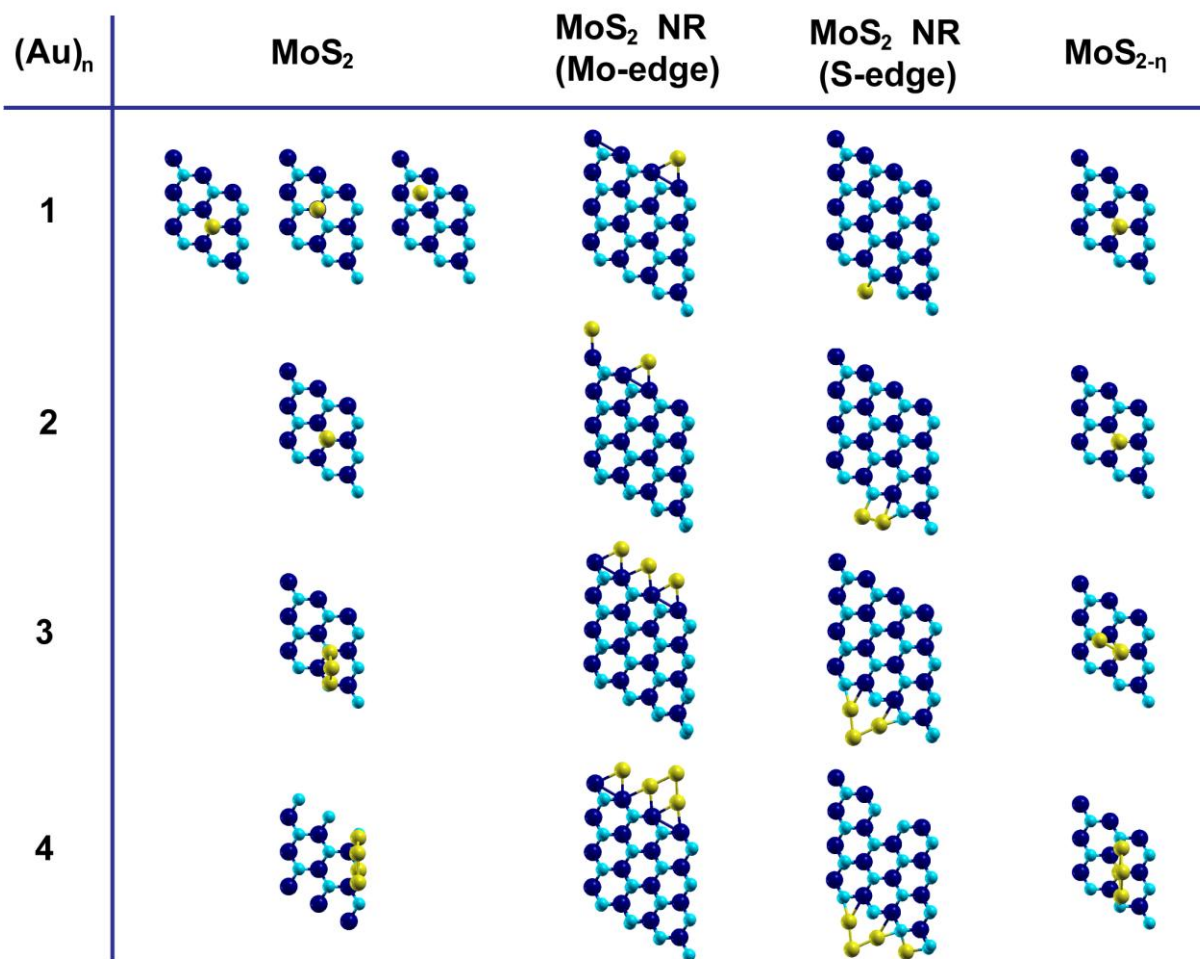
Figure S8. Adsorption configuration for 1-4 Au atoms on four different MoS_2 substrates. Mo is shown as dark blue, S as blue, and Au as gold spheres.

Supporting Note S5

The role of electron beam was analyzed by the *in situ* and *ex situ* control experiments. As $AuCl_3$ flows into the liquid cell, the electron beam irradiates the viewing area, generates solvated electrons (e_{aq}^{-}) from the solution[5,6] and thus creates a reducing environment.[7-10] The solvated electrons can reduce Au^{3+} ions to Au^0

S9

based on the following reaction $Au^{3+} + 3e_{aq}^{-} \rightarrow Au^{0}$, generating Au atoms in the solution. In this scenario, Au atoms may contribute to the growth of Au nanoparticle through conventional chemical Ostwald Ripening instead of the electrochemical Ostwald Ripening. To further understand this, *ex situ* experiments were first carried out to eliminate the influence of electron beam. The morphology of *ex situ* deposited Au nanoparticles on MoS$_2$ nanoflake is shown in Figure S9a. The HRTEM of Au nanoparticles on MoS$_2$ is shown in Figure S9b. The $(100)_{MoS2}$ with lattice spacing of 2.7 Å and $1/3(4\overline{2}\overline{2})_{Au}$ with lattice spacing of 2.5 Å can be clearly identified either from the HRTEM image or from the corresponding FFT shown in the inset. Figure S9c shows the EDS line scan data across an *ex situ* grown Au nanoparticle with the distinct energy peaks of Mo, S and Au. Second, the *in situ* control experiment was performed to further verify the formation of Au particles. An example TEM image of Au deposited on MoS$_2$ with beam blocked is shown in Figure S9d. It is obvious that the *ex situ* and *in situ* deposited Au particles on MoS$_2$ have a good agreement on the morphology. The Au particle size were analyzed and shown in Figure S9e, S9f for *ex situ* and *in situ* control experiment without electron beam irradiation, respectively. For these two cases, there is no significant difference in terms of either interior or edge particles size distribution. In comparison with *in situ* experiment, around 7% and 12% decrease of mean particle sizes on the interior and edges of MoS$_2$ can be identified. These results show that the nucleation and growth still happen without electron beam, and the trend that particles along edge are larger still valid. In addition, the slightly larger particle size both on the interior and along edges when electron beam is present suggests that the conventional chemical Ostwald Ripening may also happen due to direct reduction of Au^{3+} ions in the solution.
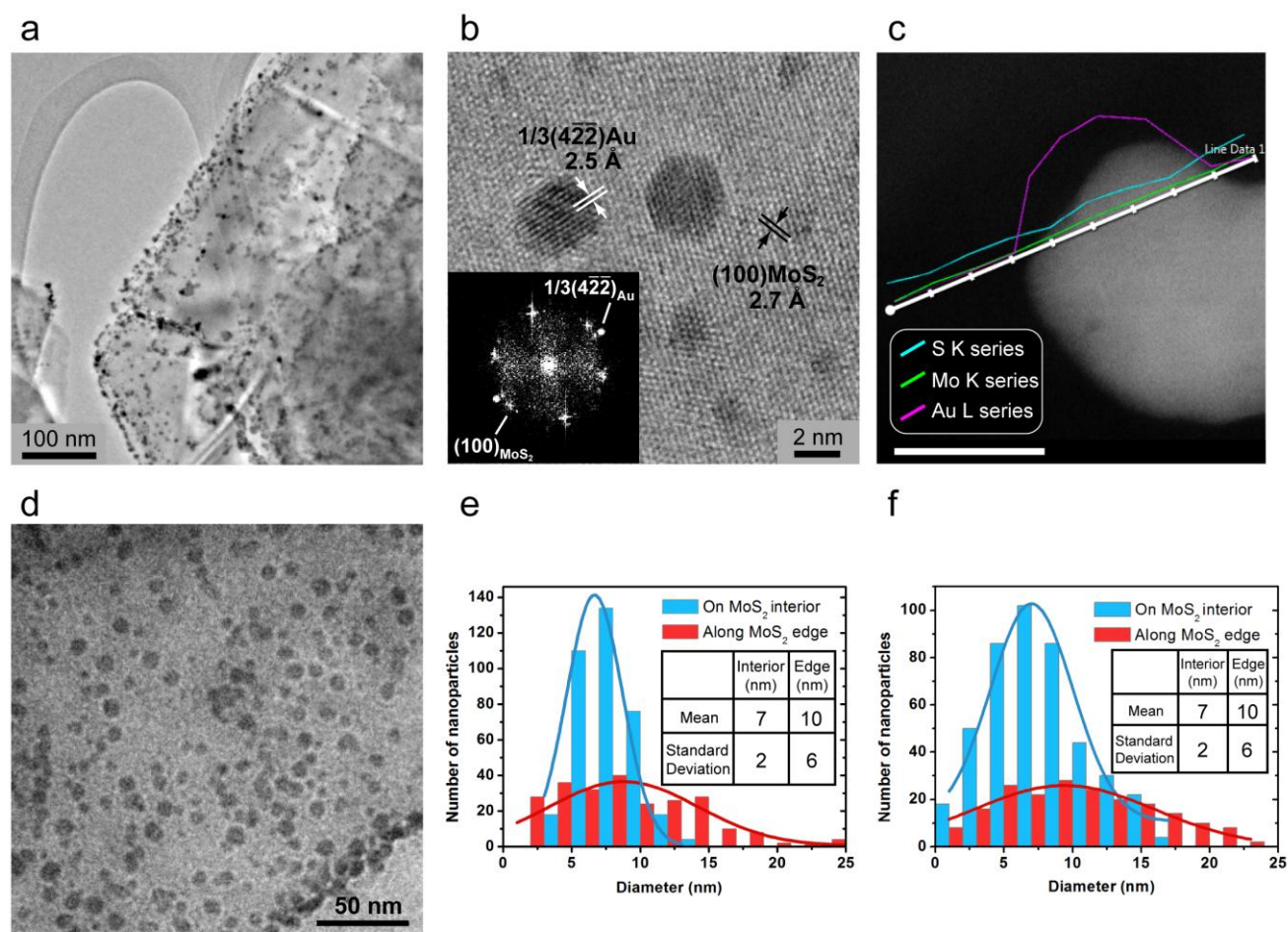
Figure S9. (**a**) TEM image of *ex situ* deposited Au nanoparticles on MoS_2. (**b**) HRTEM of *ex situ* deposited Au nanoparticles on MoS_2 nanoflake. Inset shows corresponding FFT pattern. (**c**) HAADF image of an *ex situ* deposited Au nanoparticle on MoS_2. EDS line scan data showing Mo, S, and Au peaks (signals from copper grid were excluded) that overlaid on the image. The scale bar is 10 nm. (**d**) TEM image of Au particles on MoS_2 from *in situ* control experiment without electron beam irradiation. (**e**)(**f**) Au nanoparticles size distribution and the Gaussian fitting for the conditions of *ex situ* and *in situ* control experiments without electron beam. The inset tables list calculated mean and standard deviation of Au nanoparticles diameter.

S11

References

1   T. Malis, S. Cheng and R. Egerton, *Microsc. Res. Tech.*, 1988, **8**, 193-200.

2   A. Garcia, A. M. Raya, M. M. Mariscal, R. Esparza, M. Herrera, S. I. Molina, G. Scavello, P. L. Galindo, M. Jose-Yacaman and A. Ponce, *Ultramicroscopy*, 2014, **146**, 33-38.

3   H. P. Komsa, J. Kotakoski, S. Kurasch, O. Lehtinen, U. Kaiser and A. V. Krasheninnikov, *Phys. Rev. Lett.*, 2012, **109**, 035503.

4   W. Bauer and A. Sosin, *Phys. Rev.*, 1964, **135**, A521.

5   N. M. Schneider, M. M. Norton, B. J. Mendel, J. M. Grogan, F. M. Ross and H. H. Bau, *J. Phys. Chem. C*, 2014, **118**, 22373-22382.

6   N. D. Loh, S. Sen, M. Bosman, S. F. Tan, J. Zhong, C. A. Nijhuis, P. Kral, P. Matsudaira and U. Mirsaidov, *Nat. Chem.*, 2017, **9**, 77-82.

7   T. J. Woehl, J. E. Evans, I. Arslan, W. D. Ristenpart and N. D. Browning, *ACS Nano*, 2012, **6**, 8599-8610.

8   K. Jungjohann, S. Bliznakov, P. Sutter, E. Stach and E. Sutter, *Nano Lett.*, 2013, **13**, 2964-2970.

9   J. H. Park, N. M. Schneider, J. M. Grogan, M. C. Reuter, H. H. Bau, S. Kodambaka and F. M. Ross, *Nano Lett.*, 2015, **15**, 5314-5320.

10 R. R. Unocic, A. R. Lupini, A. Y. Borisevich, D. A. Cullen, S. V. Kalinin and S. Jesse, *Nanoscale*, 2016, **8**, 15581-15588.